

Colloidal Probe Atomic Force Microscopy Reveals Anomalous Underscreening: A Matter of Experimental Conditions

Thomas Tilger,¹ Esther Ohnesorge,¹ Michalis Tsintaris,¹
Kazue Kurihara,² Hayden Robertson,^{1,*} and Regine von Klitzing^{1,†}

¹*Soft Matter at Interfaces, Department of Physics,
Technical University of Darmstadt, 64289 Darmstadt, Germany*

²*New Industry Creation Hatchery Center, Tohoku University, 980-8577 Sendai, Japan*
(Dated: March 10, 2026)

There is considerable debate about anomalous underscreening in highly concentrated electrolytes: While surface force apparatus (SFA) measurements have confirmed anomalously long screening lengths, so far they have not yet been detected in experiments using colloidal probe atomic force microscopy (CP-AFM). CP-AFM measurements across aqueous LaCl_3 solutions demonstrate that by adapting the experimental conditions to those of SFA studies, similarly large screening lengths can be achieved at high salt concentrations. This represents the first observation of anomalous underscreening with CP-AFM. These findings leave room for speculations about the ordering of the confined electrolyte.

INTRODUCTION

Electrostatic interactions and the arising electric double layer force are a cornerstone to our modern understanding of interactions in colloidal systems. According to the classical Debye-Hückel theory [1], dilute electrolytes can be described by an exponentially decaying force profile with the Debye length

$$\lambda_D = \sqrt{\frac{\epsilon_r \epsilon_0 k_B T}{2e^2 N_A I}}, \quad (1)$$

where $\epsilon_r \epsilon_0$ represents the permittivity of the medium, k_B and N_A are the Boltzmann and Avogadro constants, respectively, T is the absolute temperature, and e is the elementary charge. $I = \sum_i c_i z_i^2$ denotes the ionic strength of the electrolyte: the sum over all ionic species with the respective valences z_i and concentrations c_i . From Eq. (1), it can be seen that λ_D decreases with increasing concentration (ionic strength). In highly concentrated electrolytes, however, the underlying mean-field assumption in the Debye-Hückel theory of non-interacting ions breaks down. As initially emphasized by Kirkwood [2, 3], excluded volume effects must be accounted for at higher electrolyte concentrations, which ultimately cause the electrostatic interaction to transition from a monotonic exponential to a damped oscillatory decay. This transition at some critical concentration is known as the Kirkwood point. In this higher concentration regime, the screening ability of the electrolyte is significantly reduced compared to the Debye-Hückel predictions and the observed screening length λ_S starts to increase with concentration.

Recent studies have highlighted the ubiquitous nature of this *underscreening effect*, which commonly manifests

as re-entrant behavior with increasing electrolyte concentration [4, 5]. The extent of underscreening, however, is still under heavy debate and challenges our fundamental understanding of electrolytes [6]. Motivated by a seminal analysis by Lee *et al.* [7], the screening lengths derived from experiment and theory are often categorized according to a scaling law of type

$$\frac{\lambda_S}{\lambda_D} \sim \left(\frac{a}{\lambda_D}\right)^p, \quad (2)$$

with ion size a and exponent p . *Normal* underscreening, as deduced from the re-entrant swelling behavior of polymer brushes [8] as well as from small-angle X-ray scattering [9] and optical second harmonic scattering [10] in bulk electrolyte solutions, is characterized by an exponent $1 \leq p \leq 2$. In contrast, substantially larger screening lengths were deduced from surface force apparatus (SFA), also known as surface force balance (SFB), measurements [11–14], and studies detecting the surface-excess of fluorescein *via* fluorescence emission [15] across a variety of highly concentrated aqueous salt solutions. Comparable findings in ionic liquids [14, 16–18] indicate that these anomalously large screening lengths, coined *anomalous* underscreening, are characterized by the exponent $p = 3$ in Eq. (2), and represent a general feature of strongly correlated electrolytes under confinement.

Despite the conceptual similarities between the colloidal probe atomic force microscope (CP-AFM) and SFA, comparable long-ranged repulsive forces in highly concentrated aqueous electrolytes have not been found by AFM [19]. To date, there is only one single AFM study reporting anomalously large screening lengths, derived in an ionic liquid at elevated temperature [20]. These apparent inconsistencies between different experimental methods have stimulated extensive theoretical efforts to rationalize underscreening. Molecular dynamics simulations within the restricted primitive model have found anomalous underscreening, however, suggest that the screening length depends on a full phase diagram of

* hayden.robertson@pkm.tu-darmstadt.de

† klitzing@smi.tu-darmstadt.de

reduced temperature and reduced bulk ion number density, rather than being solely a function of a/λ_D [21]. Most recently, polarizable molecular dynamics simulations by Baker *et al.* extended preceding statistical mechanical analyses to reveal *multiple* decay modes of the electrostatic potential, each of which with its own decay length and some closely matching the experimental results [22]. That is, the authors prescribe that both *normal* and *anomalous* underscreening, along with further modes, are always present but can only be revealed by certain experimental approaches. However, further insights into why specific experiments are only sensitive to certain modes are not provided. As such, in this work we use the terms *normal* and *anomalous* strictly as operational labels, independent of their conventional meanings, to denote screening lengths governed by scaling with $p = 1 - 2$ and $p = 3$, respectively.

Herein we systematically converge the experimental conditions of the CP-AFM towards those of an SFA to demonstrate that the experimental conditions strongly influence the interactions encountered in highly concentrated electrolytes. We first revisit a conventional AFM setup and show that an increasing LaCl_3 concentration leads to a progressively stronger electrostatic screening and, at the highest concentrations, even purely attractive interactions. These results are expected and align with the Debye-Hückel theory. By then varying the size of the colloidal probe, equilibration time, and approach speed, we reveal long-ranged repulsion at high electrolyte concentrations. Finally, we present that the extracted electrostatic screening lengths follow the scaling relationship previously observed only in SFA experiments [7], indicative of anomalous underscreening.

EXPERIMENTAL SECTION

Colloidal probe atomic force microscopy (CP-AFM) measurements [23, 24] were conducted between a silica microsphere attached to a cantilever and a planar quartz substrate (Plano) in aqueous LaCl_3 (Sigma-Aldrich, 99.999%) solutions over a wide range of concentrations (0.001-1 M). Ultrapure Milli-Q water (Merck, 18.2 M Ω cm resistivity at 25 °C) was used throughout unless otherwise stated. The quartz disk was initially cleaned in a 3:1 (vol:vol) piranha solution of sulfuric acid (Carl Roth, 98%) and hydrogen peroxide (Carl Roth, 30%) for 30 min to remove any organic contaminants. The tipless cantilever (resonance frequency ≈ 40 kHz, spring constant ≈ 0.8 N/m) was initially cleaned with water and ethanol (Carl Roth, 99.9%) followed by an oxygen plasma treatment (0.4 mbar, 50 W) for 210 s. To prepare the colloidal probes, a silica microsphere was glued to the end of the cantilever (MikroMasch) with UHU PLUS ENDFEST adhesive using a micromanipulator (Sutter Instrument). The colloidal probes were then sintered at 1150 °C for 3 h; this process removes

organic contaminants which may remain from the glue and reduces the surface roughness of the microspheres [25]. Two sizes of nonporous silica microspheres were employed; their post-sintering radii were determined from scanning electron microscopy images to be $(2.1 \pm 0.1) \mu\text{m}$ (Bangs Laboratories) and $(8.5 \pm 0.1) \mu\text{m}$ (microParticles).

Prior to each measurement, the quartz disk and colloidal probe were cleaned with water and ethanol, and again treated with an oxygen plasma for 210 s. For all experiments, a temperature of 30 °C was maintained within the sample chamber of the closed-loop AFM (MFP-3D, Oxford Instruments), and the chamber was fully sealed in order to prevent evaporation of the electrolyte during the experiments. This is confirmed by the close agreement between theoretical Debye lengths λ_D and the experimentally observed screening lengths λ_S for low electrolyte concentrations. Under the experimental conditions within this work (i.e., $\text{pH} \gtrsim 3$), silica and quartz bear a negative charge due to ionization of surface silanol groups (SiO^-) [26, 27]. However, strong adsorption of the trivalent La^{3+} ions is expected to induce charge reversal in the investigated concentration range [28]. The reported interaction forces are normalized by the colloidal probe radius R according to Derjaguin's approximation $F/R(h) = 2\pi W(h)$ to obtain the interaction energy W of two planar surfaces at the same separation h [29].

RESULTS AND DISCUSSION

We begin our analysis by establishing a reference point: a standard CP-AFM setup as employed by previous investigations of electrostatic interactions in a variety of systems, ranging from simple salts to nanoparticles [30–32]. Here the radius of the colloidal probe was 2.1 μm and the equilibration time as well as the approach speed were fixed to 30 min and 200 nm/s, respectively. The data displayed in Fig. 1 (a) present the force curves obtained under these conditions. In brief, at low concentrations (*e.g.*, 0.030 M) the formation of an electric double layer repulsion is demonstrated. This repulsion then becomes suppressed as the salt concentration increases (≥ 0.500 M). At these ionic strengths, pure attractive van der Waals forces down to contact are observed as electric double layer forces are completely screened. These attractive interactions are also presented in Figure S1 (a) in the Supplemental Material [33]. We do not observe any long-ranged repulsive force that could be of electrostatic origin for concentrations ≥ 0.500 M. This is further exemplified in Fig. S2 (a) in the Supplemental Material [33]. These results are in agreement with the expectations from the canonical Debye-Hückel theory and a previous CP-AFM study on highly concentrated electrolytes [19]. This represents the current state of the art regarding the reported absence of anomalous underscreening in AFM measurements, and establishes the starting point of our efforts to adapt AFM measurements to SFA conditions.

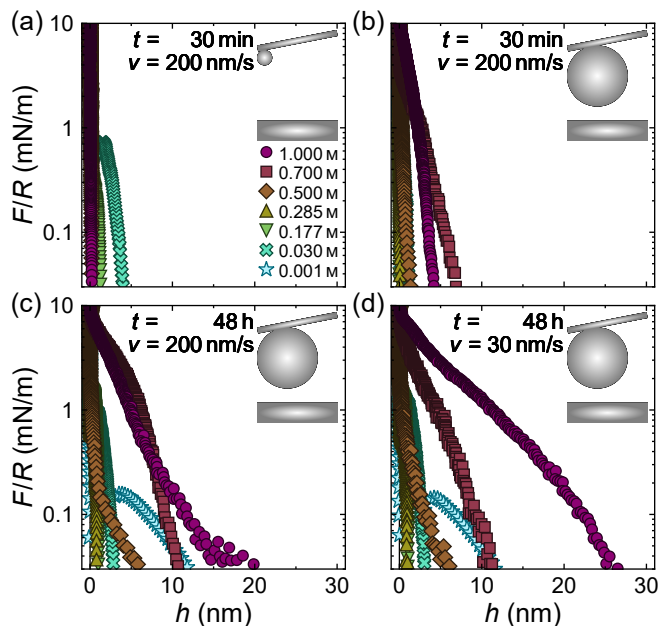


FIG. 1. Normalized interaction force F/R between a silica colloidal probe and a planar quartz substrate at separation h immersed in aqueous LaCl_3 electrolytes of various concentrations: 0.001 M, 0.030 M, 0.177 M, 0.285 M, 0.500 M, 0.700 M and 1.000 M. Top row: Data captured after an equilibration time of 30 min with an approach speed of 200 nm/s using a (a) 2.1 μm and (b) 8.5 μm colloidal probe. Bottom row: Captured with the larger 8.5 μm colloidal probe after an equilibration time of 48 h at an approach speed of (a) 200 nm/s and (b) 30 nm/s. The force profiles present an emerging repulsion in the highly concentrated regime with (a) \rightarrow (b) increasing probe size, (b) \rightarrow (c) longer equilibration time, and (c) \rightarrow (d) decreasing approach speed. A linear representation, also highlighting attractive interactions, is provided as Fig. S1 in the Supplemental Material [33].

In an effort to converge CP-AFM towards SFA, we must consider the inherent differences in measuring geometries; namely, the difference in radii of curvature between the interacting surfaces. While it is technically unfeasible to use colloidal probes with dimensions comparable to the centimeter-scale SFA cylinders, we move towards a larger contact area by increasing the probe radius from 2.1 μm to 8.5 μm . To begin, we keep the equilibration time and approach speed constant to ensure only to interrogate the geometrical influence. With a focus on higher electrolyte concentrations, moving from Fig. 1 (a) to (b) demonstrates a clear transition in the detected interaction force: from a pure attraction for the smaller colloidal probe size towards a repulsion over several nanometers for the larger probe. These results clearly contradict the Debye-Hückel predictions, which state $\lambda_D < 0.2$ nm for $c \geq 0.500$ M. We highlight that the two lowest LaCl_3 concentrations examined here (*i.e.*, 0.001 M and 0.030 M) also exhibit electrostatic repulsion as expected by Debye-Hückel theory, however, are hidden in Fig. 1 (b) due to their lower magnitude (see Fig. S2 (b) in the Supplemental

Material [33]). Therefore, a true re-entrant behavior of the electric double layer force is observed with increasing concentration.

Earlier studies have suspected a lack of sensitivity to be responsible for the absence of long-ranged repulsive forces in AFM experiments [13, 16]. The increase in colloidal probe size here indeed suppresses the noise floor in the normalized force, however, the magnitude of normalized electrostatic force encountered in SFA studies exhibiting an anomalously large electrostatic repulsion falls within the resolution of our AFM measurements [13, 14, 16, 17]. Additionally, the repulsion encountered in Fig. 1 (b) upon increasing colloidal probe size would have been clearly resolvable with the small probe in Fig. 1 (a). Therefore, we conclude that the decisive factor presented here is indeed the radius of curvature of the interacting surfaces rather than the improved force resolution.

Having examined the geometric properties, we now turn our attention to the impact of equilibration time on resultant interaction forces, as adequate equilibration is essential to minimize thermal drifts in the system. Of note, SFA experiments on diluted LaCl_3 solutions have revealed significant changes in long-ranged interactions over several hours due to slow diffusion processes [12]. Complementary measurements on highly concentrated ionic liquid/water mixtures show that the electrolyte structure near interfaces evolves over comparable timescales, altering the extent of long-range interactions [18]. Therefore, the preceding setup with the 8.5 μm colloidal probe was left to equilibrate for at least 48 h. As can be seen in Fig. 1 (c), the re-entrant behavior of the electric double layer force becomes more clearly visible. From low to intermediate electrolyte concentrations, the electric double layer repulsion is progressively screened as the salt concentration increases, up to ≈ 0.200 M. Upon further increase in LaCl_3 concentration, the range of the repulsion increases monotonically again, up to almost 20 nm at 1.000 M. As will be later discussed, for low concentrations ($c \leq 0.030$ M) the deduced screening length at the end of the experiment is in close agreement with the corresponding Debye length. This confirms that the observed increased repulsion is not due to a change in the LaCl_3 concentration within the AFM cell over the duration of the experiment. Thus, the changes in the interaction force over two days could indicate very slow ion dynamics near the interfaces; this aligns with previous findings [18]. We hypothesise that the strong ion-ion correlations in these highly concentrated LaCl_3 solutions could slow down diffusive processes close to the interfaces, resulting in the requisite longer equilibration times.

Finally, we illuminate the role of approach speed. While the electric double layer force is considered a static equilibrium force, any object moving through a fluid is also subject to dynamic viscous forces. Due to the larger geometrical dimensions which inevitably enhance hydrodynamic effects, the mica cylinders in SFA experiments

are typically moved at much slower speeds than colloidal probes: ~ 1 nm/s *vs.* ~ 200 nm/s. To mimic these conditions, the approach speed was reduced to 30 nm/s. All other parameters remained unchanged. A further reduction in approach speed was limited by the vibration isolation of the AFM, which caused a substantial increase in noise during contact. As depicted in Fig. 1 (d), the interaction is clearly altered by the reduction in approach speed. Small changes are observed at low to intermediate salt concentrations, while the main impact is exerted on the highly concentrated LaCl_3 solutions. The overall trend of re-entrant double layer repulsion is, however, reinforced.

From here, the following question is raised: to which extent is electrolyte viscosity responsible for the velocity dependence observed in our experiments? The role of viscous forces in SFA measurements has been examined in detail, with results demonstrating that the ratio between electrostatic and viscous forces scales as ηRv , with dynamic viscosity η , radius of curvature R , and approach speed v [38]. Under the experimental conditions employed in this work (*i.e.*, a temperature of 30 °C), previous investigations on the LaCl_3 electrolyte have reported a monotonic increase in viscosity with increasing concentration, with a ceiling of approximately 1.6 mPa s at 1 M [39, 40]. Importantly, this is not more than twice the viscosity of pure water. Furthermore, compared to our AFM investigations with a $R = 8.5$ μm colloidal probe approaching the surface at $v \leq 200$ nm/s, the influence of viscosity on SFA experiments ($\eta = 37$ mPa s, $R = 8.9$ mm, $v \geq 0.07$ nm/s in [38]) is at least 8 times as large. Hydrodynamic forces arising from fluid drainage can therefore be neglected for the experiments presented here at 200 nm/s. The changes observed upon reducing the approach speed must originate from mechanisms beyond simple viscous drag, which would instead predict stronger repulsion at higher approach speeds. We propose that the emergence of long-ranged repulsive interactions requires the presence of an equilibrated ionic structure in the vicinity of the interfaces, which is perturbed if the interfaces approach too fast. Observations of ordered structure formation in confined ionic liquids support this interpretation [41–44]. Consequently, we hypothesize that the slowest approach speed most closely approximates equilibrium conditions and should therefore be considered.

To this point, we have systematically converged the experimental conditions of our CP-AFM setup toward those of an SFA. In doing so, we have successfully shown the crucial impact of these measurement conditions on the interactions observed in highly concentrated electrolyte solutions. We have demonstrated that by using a large colloidal probe, long equilibration times, and slow approach speeds, CP-AFM is capable of detecting long-ranged repulsive forces similar to the SFA. Specifically, we hypothesize that La^{3+} and Cl^- ions progressively adsorb at the quartz-electrolyte interface, establishing a re-

pulsive structure that can be readily disrupted by faster movements and abrupt hydrodynamic drainage. Importantly, the sensitivity to this ionic structure appears to increase with larger contact area. Accordingly, we emphasize that none of the aforementioned parameters alone are responsible for the emergent repulsion at high concentrations. Rather, the synergy of all parameters generates the observed long-ranged repulsive forces. This is further exemplified in Fig. S3 in the Supplemental Material [33], demonstrating the absence of repulsive interactions for the small colloidal probe under the same conditions that were identified for the large probe in Fig. 1 (d).

We now turn to extract the corresponding screening lengths from Fig. 1 (d). To do so, the data at separation h was modeled according to the classical theory of Derjaguin, Landau, Verwey, and Overbeek (DLVO) [45–47] as a superposition of the non-retarded van der Waals (vdW) attraction [48]

$$\frac{F_{\text{vdW}}}{R} = -\frac{H}{6h^2} \quad (3)$$

and the electric double layer (EDL) repulsion within the Debye-Hückel approximation [49]

$$\frac{F_{\text{EDL}}}{R} = 4\pi\epsilon_r\epsilon_0 \frac{\psi_{\text{eff}}^2}{\lambda_S} e^{-\frac{h}{\lambda_S}}. \quad (4)$$

The Hamaker constant $H = (2.25 \pm 0.50) \times 10^{-21}$ J was chosen in accordance with the literature [25]. Similarly, the concentration-dependent relative permittivity ϵ_r was determined from literature values (see the Supplemental Material [33] for further details). The effective potential ψ_{eff} and screening length λ_S were extracted from model fits to the data. In line with literature, an additional non-DLVO attraction $A_{\text{att}} \exp(h/\lambda_{\text{att}})$ with amplitude $A_{\text{att}} = -0.8$ mN/m and decay length $\lambda_{\text{att}} = 1.3$ nm was introduced at the lowest LaCl_3 concentration (0.001 M) to model the data [30]. The origin of this attraction has been attributed to ion-ion correlation effects, possibly with additional contributions from surface charge heterogeneities and charge fluctuation forces [30].

Figure 2 (a) presents the observed screening length λ_S as a function of LaCl_3 concentration and mirrors the non-monotonic behavior observed in the force curves from Fig. 1 (d). To facilitate direct comparison with salts of different valences, the ionic strength I is also provided ($I = 6c$ for a 1:3 electrolyte). At low to intermediate electrolyte concentrations, λ_S decreases monotonically in close agreement with the Debye length λ_D . However, as the electrolyte concentration increases above ≈ 0.200 M, a monotonic increase in λ_S is observed. At these higher concentrations, λ_S exceeds λ_D by several nanometers and also surpasses the screening lengths obtained in the mM range, despite the 1000-fold higher concentration.

Finally, we place our findings in a broader context through a scaling analysis of the extracted screening lengths. SFA measurements have consistently demonstrated that the screening length across aqueous solutions of various alkali halides and also ionic liquids can

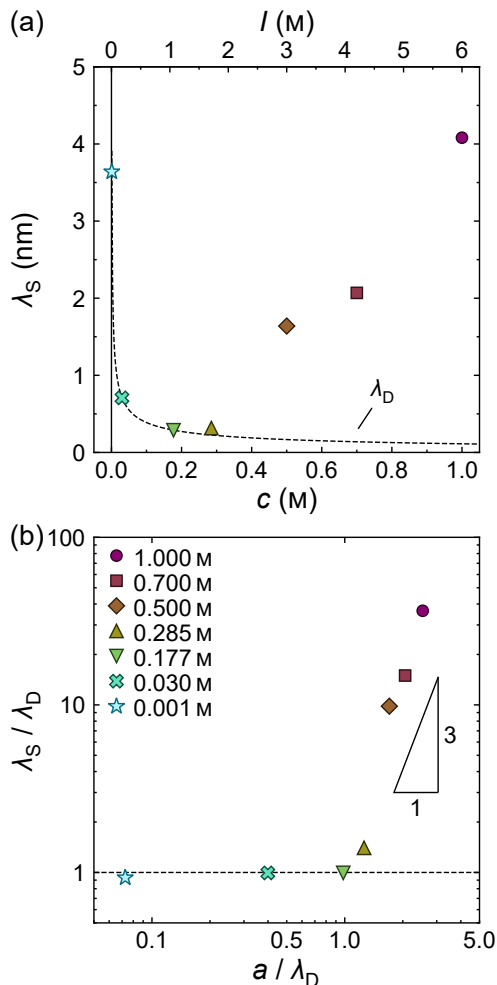


FIG. 2. The experimental screening length λ_s in aqueous LaCl_3 electrolytes as extracted from the data presented in Fig. 1 (d). (a) Screening length as a function of concentration c and ionic strength $I = 6c$. The dashed black line presents the predictions of the Debye-Hückel theory. (b) Screening length λ_s normalized by the Debye length λ_D as a function of the normalized mean ion size a/λ_D . The black triangle denotes the slope predicted by the scaling law from Eq. (2) for $p = 3$, indicative of anomalous underscreening. A linear representation of these data and a superimposed model fit of the scaling law are presented in Fig. S4 in the Supplemental Material [33].

be normalized to collapse onto a single curve [7, 14, 18], which is described by the universal scaling relationship expressed in Eq. (2) with $p = 3$ [7]. This is in contrast to other investigations which align with $p \leq 2$ [8–10]. To test the validity of the scaling law for our dataset, we normalize the calculated screening length by the Debye length given in Eq. (1). Similarly, the normalized ion size a/λ_D is derived from the mean ion size $a = 2.842 \text{ \AA}$ of the electrolyte, as estimated from the tabulated radii of La^{3+} and Cl^- [50]. As illustrated by the slope of the black triangle in Fig. 2 (b) the data presented in this work are indeed consistent with the proposed scaling law for

anomalous underscreening from Eq. (2) with $p = 3$. A visualization of the smaller scaling exponents $p = 1 - 2$, as expected for *normal* underscreening, is given in Fig. S4 in the Supplemental Material [33] and emphasizes that the depicted increase in screening length here clearly goes beyond *normal* underscreening. The onset of the increase in screening length in Fig. 2 (b) coincides with $\lambda_D \approx a$, highlighting the remarkable similarity between the AFM results presented herein and prior SFA investigations.

Of note, this similarity differentiates our work from previous AFM investigations [19] that could not confirm the anomalously large screening lengths observed in SFA experiments. Molecular dynamics simulations have already suggested that the screening length in electrolytes in bulk is not solely a function of a/λ_D , but depends on a full phase diagram of reduced temperature and reduced ion number density [21]. Our results extend this picture and reveal that additional factors have to be taken into account for experimental realizations probing the screening length that involve, *e.g.*, interfaces. Most recently, Fourier analysis on radial charge density profiles extracted from a new set of molecular dynamics simulations has shown the presence of multiple screening modes in aqueous electrolytes. At low concentrations, a single monotonic decay dominates, while at higher concentrations oscillatory modes with distinct characteristic decay lengths emerge, some of which align with screening lengths observed in experiments [22]. Our findings complement this theoretical analysis and provide the first insights into which physical parameters actually determine the emergence of specific decay modes in experiments.

CONCLUSION

In the present work, we have demonstrated through colloid-probe atomic force microscopy measurements that interactions in highly concentrated aqueous LaCl_3 electrolytes are not governed exclusively by salt concentration. Additional parameters of the experimental setup, such as the size of the interacting surfaces, decisively control the emergence and magnitude of re-entrant electric double layer forces. By converging the experimental conditions of AFM towards those of the SFA, we have systematically tuned the interaction from purely attractive van der Waals forces to long-ranged repulsive double layer forces. Notably, at higher electrolyte concentrations, the range of the repulsion increased and the extracted screening lengths followed the universal scaling law previously inferred from SFA experiments [7]. Thus, our results mark the first experimental observation of anomalously large screening lengths (*i.e.*, $p = 3$) in aqueous electrolytes with the AFM, challenging former beliefs that the AFM is *inherently* unable to detect anomalous underscreening. Rather, our findings support the interpretation of recent computational work: that previous AFM investigations explored only parts of an

experimental parameter space that favored attractive interactions. Taken together, this work highlights avenues for systematically controlling the strength of the repulsive double layer forces in highly concentrated aqueous electrolyte solutions.

H. R. gratefully acknowledges a Humboldt Research Fellowship from the Alexander von Humboldt Stiftung.

-
- [1] P. Debye and E. Hückel, Zur Theorie der Elektrolyte: I. Gefrierpunktserniedrigung und verwandte Erscheinungen, *Phys. Z.* **24**, 185 (1923).
- [2] J. G. Kirkwood, Statistical mechanics of liquid solutions, *Chem. Rev.* **19**, 275 (1936).
- [3] J. G. Kirkwood and J. C. Poirier, The statistical mechanical basis of the Debye-Hückel theory of strong electrolytes, *J. Phys. Chem.* **58**, 591 (1954).
- [4] H. Yuan, W. Deng, X. Zhu, G. Liu, and V. S. J. Craig, Colloidal systems in concentrated electrolyte solutions exhibit re-entrant long-range electrostatic interactions due to underscreening, *Langmuir* **38**, 6164 (2022).
- [5] G. S. Dunlop, H. Robertson, Z. Di Pietro, S. W. Prescott, A. R. J. Nelson, V. S. J. Craig, E. J. Wanless, and G. B. Webber, Strong anionic polyelectrolyte brush exhibits specific ion dependent brush re-swelling in hypersaline conditions, *J. Colloid Interface Sci.* **703**, 139233 (2026).
- [6] G. R. Elliott, K. P. Gregory, H. Robertson, V. S. Craig, G. B. Webber, E. J. Wanless, and A. J. Page, The known-unknowns of anomalous underscreening in concentrated electrolytes, *Chem. Phys. Lett.* **843**, 141190 (2024).
- [7] A. A. Lee, C. S. Perez-Martinez, A. M. Smith, and S. Perkin, Scaling analysis of the screening length in concentrated electrolytes, *Phys. Rev. Lett.* **119**, 1 (2017).
- [8] H. Robertson, G. R. Elliott, A. R. J. Nelson, A. P. Le Brun, G. B. Webber, S. W. Prescott, V. S. J. Craig, E. J. Wanless, and J. D. Willott, Underscreening in concentrated electrolytes: Re-entrant swelling in polyelectrolyte brushes, *Phys. Chem. Chem. Phys.* **25**, 24770 (2023).
- [9] M. Dinpajoo, E. Biasin, E. T. Nienhuis, S. T. Mergelsberg, C. J. Benmore, G. K. Schenter, J. L. Fulton, S. M. Kathmann, and C. J. Mundy, Detecting underscreening and generalized Kirkwood transitions in aqueous electrolytes, *J. Chem. Phys.* **161**, 10.1063/5.0234518 (2024).
- [10] F. Rondepierre, P.-F. Brevet, and J. Duboisset, Asymptotic underscreening in concentrated electrolytes measured by optical second harmonic scattering of water, *J. Phys. Chem. Lett.* **16**, 2690 (2025).
- [11] R. Pashley and J. Israelachvili, DLVO and hydration forces between mica surfaces in Mg^{2+} , Ca^{2+} , Sr^{2+} , and Ba^{2+} chloride solutions, *J. Colloid Interface Sci.* **97**, 446 (1984).
- [12] R. Pashley, Forces between mica surfaces in La^{3+} and Cr^{3+} electrolyte solutions, *J. Colloid Interface Sci.* **102**, 23 (1984).
- [13] T. Baimpos, B. R. Shrestha, S. Raman, and M. Valtiner, Effect of interfacial ion structuring on range and magnitude of electric double layer, hydration, and adhesive interactions between mica surfaces in 0.05-3 M Li^+ and Cs^+ electrolyte solutions, *Langmuir* **30**, 4322 (2014).
- [14] A. M. Smith, A. A. Lee, and S. Perkin, The electrostatic screening length in concentrated electrolytes increases with concentration, *J. Phys. Chem. Lett.* **7**, 2157 (2016).
- [15] P. Gaddam and W. Ducker, Electrostatic screening length in concentrated salt solutions, *Langmuir* **35**, 5719 (2019).
- [16] M. A. Gebbie, M. Valtiner, X. Banquy, E. T. Fox, W. A. Henderson, and J. N. Israelachvili, Ionic liquids behave as dilute electrolyte solutions, *PNAS* **110**, 9674 (2013).
- [17] M. A. Gebbie, H. A. Dobbs, M. Valtiner, and J. N. Israelachvili, Long-range electrostatic screening in ionic liquids, *PNAS* **112**, 7432 (2015).
- [18] Y. K. C. Fung and S. Perkin, Structure and anomalous underscreening in ethylammonium nitrate solutions confined between two mica surfaces, *Faraday Discuss.* **246**, 370 (2023).
- [19] S. Kumar, P. Cats, M. B. Alotaibi, S. C. Ayirala, A. A. Yousef, R. van Roij, I. Siretanu, and F. Mugele, Absence of anomalous underscreening in highly concentrated aqueous electrolytes confined between smooth silica surfaces, *J. Colloid Interface Sci.* **622**, 819 (2022).
- [20] N. Hjalmarsson, R. Atkin, and M. W. Rutland, Switchable long-range double layer force observed in a protic ionic liquid, *Chem. Commun.* **53**, 647 (2017).
- [21] A. Härtel, M. Bültmann, and F. Coupette, Anomalous underscreening in the restricted primitive model, *Phys. Rev. Lett.* **130**, 108202 (2023).
- [22] S. Baker, G. R. Elliott, E. J. Wanless, G. B. Webber, V. S. J. Craig, and A. J. Page, A multimodal screening length analysis of concentrated electrolytes, *J. Colloid Interface Sci.* **709**, 139953 (2026).
- [23] H.-J. Butt, Measuring electrostatic, van der Waals, and hydration forces in electrolyte solutions with an atomic force microscope, *Biophys. J.* **60**, 1438 (1991).
- [24] W. A. Ducker, T. J. Senden, and R. M. Pashley, Direct measurement of colloidal forces using an atomic force microscope, *Nature* **353**, 239 (1991).
- [25] V. Valmacco, M. Elzbiaciak-Wodka, C. Besnard, P. Maroni, G. Trefalt, and M. Borkovec, Dispersion forces acting between silica particles across water: influence of nanoscale roughness, *Nanoscale Horiz.* **1**, 325 (2016).
- [26] R. K. Iler, *The chemistry of silica: Solubility, polymerization, colloid and surface properties, and biochemistry* (John Wiley and Sons Inc, New York, NY, 1979).
- [27] M. Kosmulski, The pH dependent surface charging and points of zero charge. X. Update, *Adv. Colloid Interface Sci.* **319**, 102973 (2023).
- [28] K. Besteman, M. A. G. Zevenbergen, H. A. Heering, and S. G. Lemay, Direct observation of charge inversion by multivalent ions as a universal electrostatic phenomenon, *Phys. Rev. Lett.* **93**, 1 (2004).
- [29] B. Derjaguin, Untersuchungen über die Reibung und Adhäsion, IV, *Kolloid-Z.* **69**, 155 (1934).
- [30] V. Valmacco, M. Elzbiaciak-Wodka, D. Herman, G. Trefalt, P. Maroni, and M. Borkovec, Forces between silica particles in the presence of multivalent cations, *J. Colloid Interface Sci.* **472**, 108 (2016).
- [31] A. M. Smith, P. Maroni, G. Trefalt, and M. Borkovec, Unexpectedly large decay lengths of double-layer forces in solutions of symmetric, multivalent electrolytes, *J. Phys. Chem. B* **123**, 1733 (2019).
- [32] M. Ludwig and R. von Klitzing, Untangling superposed double layer and structural forces across confined nanoparticle suspensions, *Phys. Chem. Chem. Phys.* **23**, 1325 (2021).
- [33] See Supplemental Material for additional representations of the force spectroscopy data, a fit to the scaling law,

- and the relative permittivity of the electrolyte solutions, which includes Refs. [34-37].
- [34] J. B. Hasted, D. M. Ritson, and C. H. Collie, Dielectric properties of aqueous ionic solutions. Parts I and II, *J. Chem. Phys.* **16**, 1 (1948).
- [35] J. Wyman and E. N. Ingalls, The dielectric constant of deuterium oxide, *J. Am. Chem. Soc.* **60**, 1182 (1938).
- [36] C. G. Malmberg and A. A. Maryott, Dielectric constant of water from 0° to 100° C, *J. Res. Natl. Bur. Stand.* **56**, 1 (1956).
- [37] M. Uematsu and E. U. Franck, Static dielectric constant of water and steam, *J. Phys. Chem. Ref. Data* **9**, 1291 (1980).
- [38] R. Lhermerout and S. Perkin, Nanoconfined ionic liquids: Disentangling electrostatic and viscous forces, *Phys. Rev. Fluids* **3**, 014201 (2018).
- [39] T. Isono, Density, viscosity, and electrolytic conductivity of concentrated aqueous electrolyte solutions at several temperatures. Alkaline-earth chlorides, lanthanum chloride, sodium chloride, sodium nitrate, sodium bromide, potassium nitrate, potassium bromide, and cadmium nitrate, *J. Chem. Eng. Data* **29**, 45 (1984).
- [40] Y.-S. Liu, Y.-F. Hu, Q.-C. Hao, X.-M. Zhang, Z.-C. Liu, and J.-G. Li, Viscosity and density of the system NaCl + LaCl₃ + H₂O and its binary subsystems at different temperatures, *J. Chem. Eng. Data* **54**, 739 (2009).
- [41] K. Ueno, M. Kasuya, M. Watanabe, M. Mizukami, and K. Kurihara, Resonance shear measurement of nanoconfined ionic liquids, *Phys. Chem. Chem. Phys.* **12**, 4066 (2010).
- [42] F. F. Canova, H. Matsubara, M. Mizukami, K. Kurihara, and A. L. Shluger, Shear dynamics of nanoconfined ionic liquids, *Phys. Chem. Chem. Phys.* **16**, 8247 (2014).
- [43] F. Federici Canova, M. Mizukami, T. Imamura, K. Kurihara, and A. L. Shluger, Structural stability and polarization of ionic liquid films on silica surfaces, *Phys. Chem. Chem. Phys.* **17**, 17661 (2015).
- [44] K. Tomita, M. Mizukami, S. Nakano, N. Ohta, N. Yagi, and K. Kurihara, X-ray diffraction and resonance shear measurement of nano-confined ionic liquids, *Phys. Chem. Chem. Phys.* **20**, 13714 (2018).
- [45] B. V. Derjaguin, A theory of interaction of particles in presence of electric double layers and the stability of lyophobic colloids and disperse systems, *Acta Phys. Chim.* **10**, 333 (1939).
- [46] Derjaguin, B. V., L. Landau, Theory of the stability of strongly charged lyophobic sols and of the adhesion of strongly charged particles in solutions of electrolytes, *Acta Phys. Chim.* **14**, 633 (1941).
- [47] E. J. W. Verwey and J. Th. G. Overbeek, *Theory of the stability of lyophobic colloids: The interaction of particles having an electric double layer.* (Elsevier Pub. Co., Amsterdam, 1948).
- [48] H. C. Hamaker, The London - van der Waals attraction between spherical particles, *Physica* **4**, 1058 (1937).
- [49] H.-J. Butt and M. Kappl, *Surface and Interfacial Forces*, 2nd ed. (Wiley-VCH Verlag GmbH & Co. KGaA, Weinheim, 2018).
- [50] R. D. Shannon, Revised effective ionic radii and systematic studies of interatomic distances in halides and chalcogenides, *Acta Cryst A* **32**, 751 (1976).

**Supplemental Material for “Colloidal Probe Atomic Force
Microscopy Reveals Anomalous Underscreening:
A Matter of Experimental Conditions”**

Thomas Tilger,¹ Esther Ohnesorge,¹ Michalis Tsintsaris,¹
Kazue Kurihara,² Hayden Robertson,^{1,*} and Regine von Klitzing^{1,†}

¹*Soft Matter at Interfaces, Department of Physics,
Technical University of Darmstadt, 64289 Darmstadt, Germany*

²*New Industry Creation Hatchery Center,
Tohoku University, 980-8577 Sendai, Japan*

(Dated: March 10, 2026)

* hayden.robertson@pkm.tu-darmstadt.de

† klitzing@smi.tu-darmstadt.de

ADDITIONAL REPRESENTATIONS OF THE FORCE SPECTROSCOPY DATA

In this section we present additional representations of the force spectroscopy data shown in the main text. Fig. S1 displays a linear representation of Fig. 1 to highlight the attractive interactions in aqueous LaCl_3 solutions that are obscured on a logarithmic y -axis.

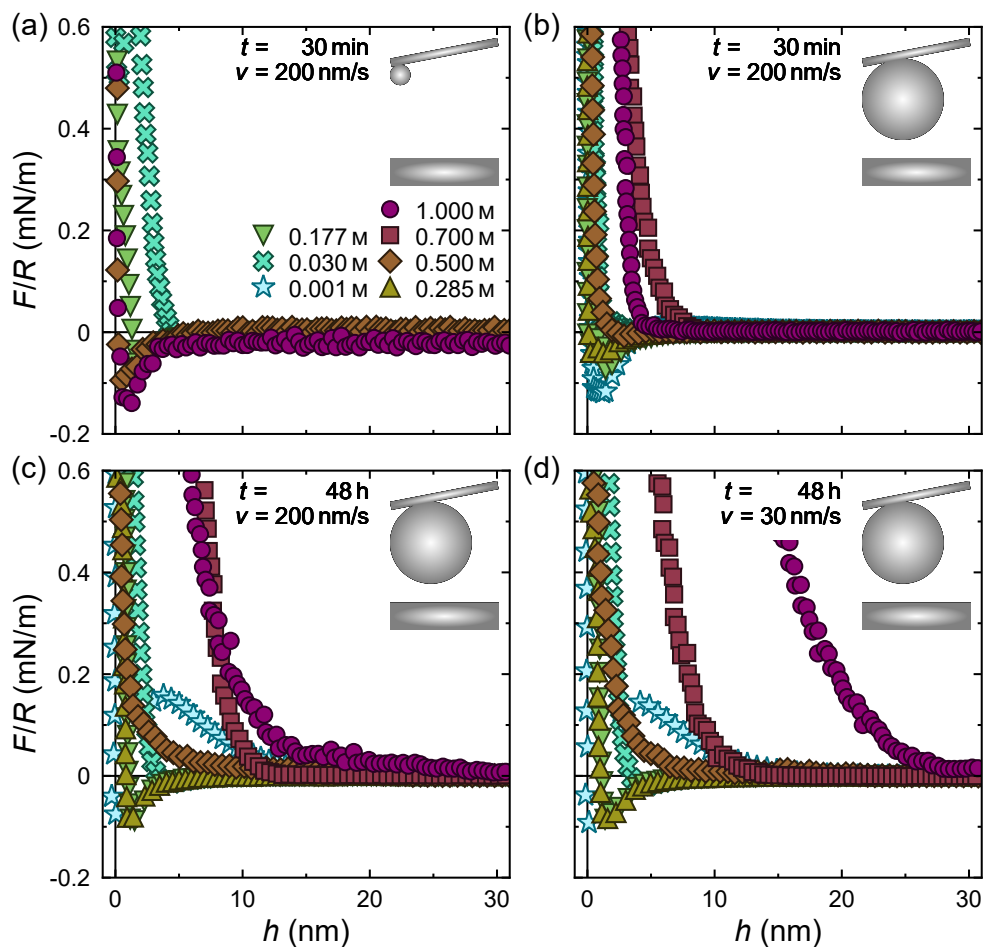


FIG. S1. Normalized interaction force F/R between a silica colloidal probe and a planar quartz substrate at separation h immersed in aqueous LaCl_3 electrolytes of various concentrations: 0.001 M, 0.030 M, 0.177 M, 0.285 M, 0.500 M, 0.700 M and 1.000 M. Top row: Data captured after an equilibration time of 30 min with an approach speed of 200 nm/s using a (a) 2.1 μm and (b) 8.5 μm colloidal probe. Bottom row: Captured with the larger 8.5 μm colloidal probe after an equilibration time of 48 h at an approach speed of (a) 200 nm/s and (b) 30 nm/s. This figure is a linear representation of Fig. 1 in the main text and visualizes attractive interactions.

The following Fig. S2 (a) presents a narrower x -range relative to Fig. 1 (a) to emphasize the decreasing range of electrostatic repulsion with increasing concentration; this is in agreement with Debye–Hückel theory. Figure S2 (b) extends the y -range of Fig. 1 (b) to highlight the weak electrostatic repulsion at the two lowest concentrations, 0.001 M and 0.030 M, revealing a clear re-entrant behavior of the electric double-layer force.

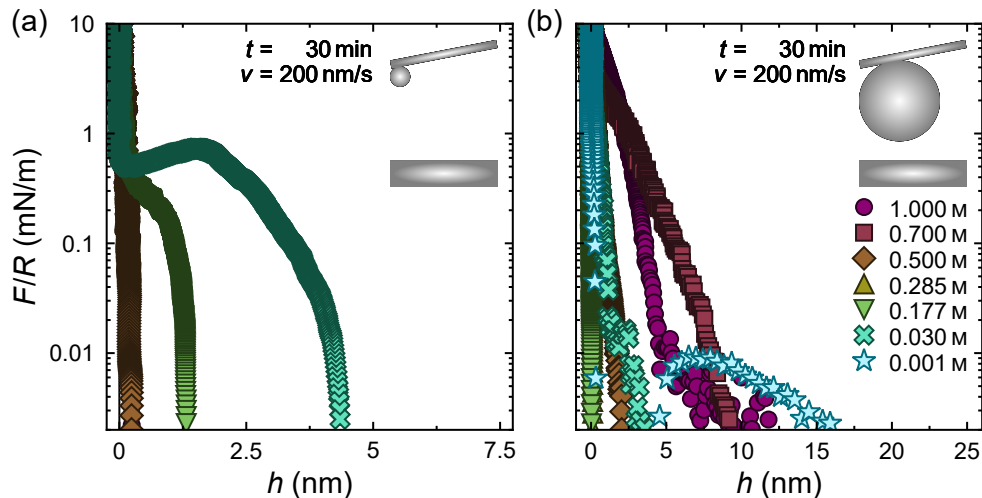


FIG. S2. Normalized interaction force F/R between a silica colloidal probe and a planar quartz substrate at separation h immersed in aqueous LaCl_3 electrolytes of various concentrations: 0.001 M, 0.030 M, 0.177 M, 0.285 M, 0.500 M, 0.700 M and 1.000 M. The data were captured after an equilibration time of 30 min with an approach speed of 200 nm/s using a (a) 2.1 μm and (b) 8.5 μm colloidal probe. This figure is identical to Fig. 1 (a) and (b) in the main text, but provides modified axes ranges.

One key outcomes from these investigations is that size of the colloidal probe, equilibration time, or approach speed alone do not control the emergence or magnitude of repulsive interactions at high LaCl_3 concentrations. Rather, the synergy of these parameters governs the repulsive interactions. To illustrate the interplay of these parameters, Fig. S3 demonstrates the absence of repulsive interactions for the small colloidal probe under the same conditions that produced clear long-ranged repulsion for the large probe in Fig. 1 (d).

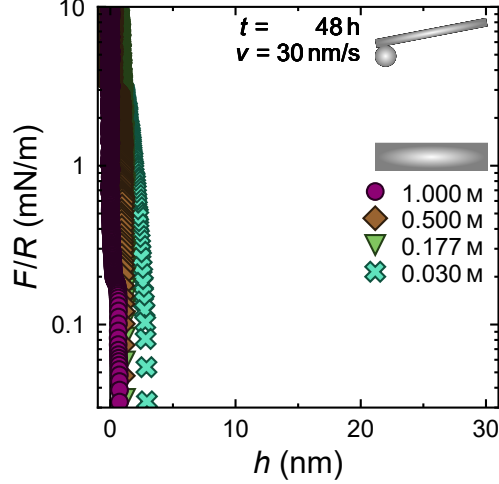


FIG. S3. Normalized interaction force F/R between the smaller silica colloidal probe with a radius of $2.1\ \mu\text{m}$ and a planar quartz substrate at separation h immersed in aqueous LaCl_3 electrolytes of various concentrations: $0.030\ \text{M}$, $0.177\ \text{M}$, $0.500\ \text{M}$ and $1.000\ \text{M}$. The data were captured after an equilibration time of $48\ \text{h}$ with an approach speed of $30\ \text{nm/s}$. This figure is shown for direct comparison with Fig. 1 (d) in the main text.

SCALING LAW

Motivated by the seminal analysis of Lee *et al.* [1], experimental screening lengths are often categorized according to the scaling law given in Eq. (2) in the main text. Anomalous underscreening is characterized by a scaling exponent $p = 3$. Therefore, we have examined the validity of the relation

$$\frac{\lambda_S}{\lambda_D} = A \left(\frac{a}{\lambda_D} \right)^3 + B \quad (\text{S1})$$

for the data presented here. Figure S4 shows the good agreement between Eq. (S1) with $A = 2.15$ and $B = -0.70$ (solid black line) and the experimental data for $a/\lambda_D > 1$. It can be seen that our measured screening lengths are compatible with *anomalous* underscreening, but clearly go beyond *normal* underscreening, as is characterized by $p = 1$ (light gray dotted line) to $p = 2$ (dark gray dash-dotted line).

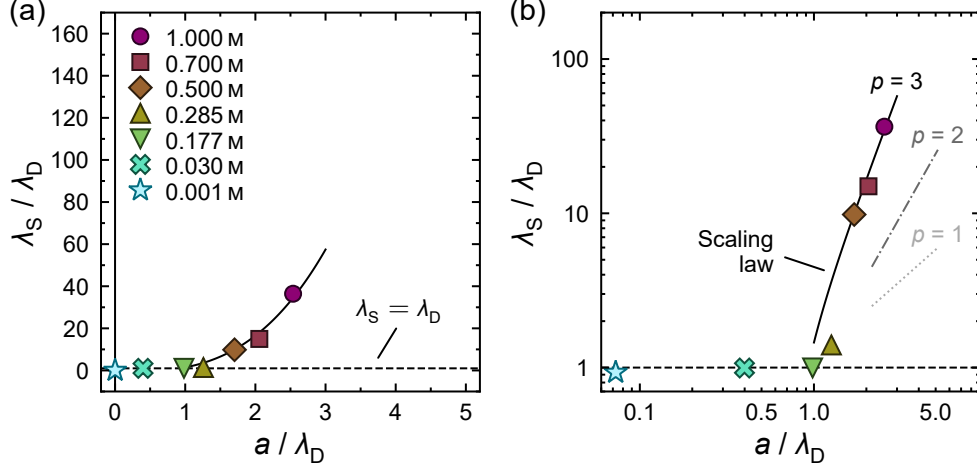


FIG. S4. The experimental screening length λ_S , normalized by the Debye length λ_D , plotted against the normalized mean ion size a/λ_D in (a) linear and (b) logarithmic representation (*c.f.* Fig. 2 in the main text). The black solid line shows the scaling law from Eq. (S1), indicative for *anomalous* underscreening, drawn for the parameters $A = 2.15$ and $B = -0.70$. The dark gray dash-dotted and light gray dotted lines denote the upper and lower bounds of the slope expected for *normal* underscreening, respectively.

RELATIVE PERMITTIVITY OF THE ELECTROLYTE SOLUTIONS

In the concentration regime investigated (up to 1 M), the addition of LaCl_3 leads to a decrease in the relative permittivity ϵ_r [2]. This reduction in ϵ_r directly enters the calculation of the Debye length in Eq. (1) of the main text and must therefore be taken into account for a quantitative analysis of the screening length. As can be seen in Fig. S5, we estimated the concentration dependence of the relative permittivity via a linear interpolation to literature data for pure water and aqueous LaCl_3 solutions of known concentration, yielding

$$\epsilon_r(c) = 76.55 - 14.10c. \quad (\text{S2})$$

To account for the elevated experimental temperature (30 °C compared to 25 °C), the literature values for non-vanishing LaCl_3 concentrations were reduced by an offset of 1.7 units, in line with the known temperature-induced change for water.

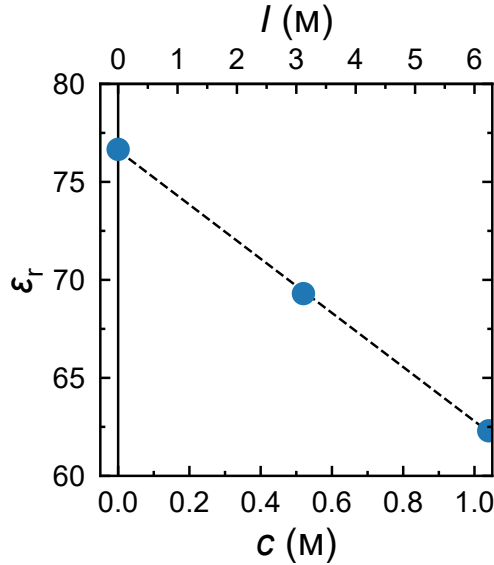


FIG. S5. Relative permittivity ϵ_r of aqueous LaCl_3 solutions at 30°C as a function of concentration c and ionic strength I (blue circles). The permittivity for pure water at was averaged from ref. [3–5]. The values for finite salt concentration were taken from ref. [2] and corrected for temperature. The black dashed line indicates a linear model to the literature values.

-
- [1] A. A. Lee, C. S. Perez-Martinez, A. M. Smith, and S. Perkin, Scaling analysis of the screening length in concentrated electrolytes, *Phys. Rev. Lett.* **119**, 1 (2017).
- [2] J. B. Hasted, D. M. Ritson, and C. H. Collie, Dielectric properties of aqueous ionic solutions. Parts I and II, *J. Chem. Phys.* **16**, 1 (1948).
- [3] J. Wyman and E. N. Ingalls, The dielectric constant of deuterium oxide, *J. Am. Chem. Soc.* **60**, 1182 (1938).
- [4] C. G. Malmberg and A. A. Maryott, Dielectric constant of water from 0° to 100°C , *J. Res. Natl. Bur. Stand.* **56**, 1 (1956).
- [5] M. Uematsu and E. U. Franck, Static dielectric constant of water and steam, *J. Phys. Chem. Ref. Data* **9**, 1291 (1980).